Industrial Engineering Journal
ISSN: 0970-2555
Volume : 51, Issue 04, April : 2022

Investigation of Parameters and Economic Efficiency Optimization for Wide-Band Fiber Laser Laser Cladding

1*Dr.Sunita Bal & 2*Dr.Jyotirmaya Satapathy

[1*] Assistant Professor, Department of Basic Science and Humanities , Nalanda Institute of Technology, Bhubaneswar, Odisha, India

[2]Assistant Professor, Department of Basic Science and Humanities, Nalanda Institute of Technology, Bhubaneswar, Odisha, India

*Corresponding author e-mail: sunitabal@thenalanda.com
jyotirmayasatpathy@thenalanda.com

Abstract

With the aim of investigating the cladding geometry characteristics by a wide-band fiber laser with coaxial rectangular nozzle, and optimizing the powder efficiency and deposition speed for economy efficiency, Fe-based alloy powder was deposited on AISI 1045 substrate by a 3000 W fiber laser in this study. Laser power (P), scan speed (V), and powder feed rate (F) were selected for a factorial design. The efects of the three process parameters on the geometry characteristics and economic efficiency of single tracks were statistically analyzed, and a linear regression model was established between the combined parameters and the relevant characteristics (including track height, ratio of track width to height, powder efficiency, and deposition speed). A process map was developed with the track shape and key economic indexes as boundaries. A flat-top feature of the track profile was found and can be utilized to achieve good cladding evenness. The process map showed that the powder efficiency and deposition speed were higher than 50% and 20 mm^3/s, respectively, when selecting process parameters in the as-built operation window.

1. Introduction

Laser cladding technology coats materials on substrates via a high-energy laser beam for the aim of surface modification. The process has more advantages than other surface modification technologies due to its concentrated energy, small heat-afected zone (HAZ), and rapid solidification; thus, small thermal deformation and a fine microstructure can be achieved. The CO_2 laser has high output power and has been applied to laser cladding for many years, but its wavelength is hard to absorb for metal materials [1]. YAG solid lasers have good performance for metal processing but low photoelectric efficiency. High-power diode lasers have been studied in recent years due to their fast deposition speed and low dilution [1–3]. Fiber laser pumped by a semiconductor diode has a high photoelectric efficiency and good beam quality; it is mainly used for elaborate processing with low power. However, there is little research on high-energy fiber may be influenced by scanning direction and have an asymmetric track; a coaxially symmetrical powder nozzle can solve these deficiencies [6, 7].

Laser cladding should ensure cladding quality and geometric accuracy. Many studies concentrated on revealing the influences of process parameters on cladding characteristics. Goodarzi et al. [7] found that the shape of the melted substrate was afected by the powder feed rate; a deep and symmetric melt zone could be generated by a low powder feed rate, and vice versa. They also revealed that laser power was the main factor afecting the melting area of the substrate. Lots of studies have found that track width increases as the power increases and track height increases as the scan speed decreases or the powder feed rate increases [8, 9]. Small laser scanning distances can generate homogeneous dilution and a small HAZ; a lower laser focus gap can obtain shallower dilution depths; and P and F have significant influences on dilution [10, 11].

Industrial Engineering Journal
ISSN: 0970-2555
Volume : 51, Issue 04, April : 2022

Many studies concentrated on process parameters P, V, and F with great interest [13]. Exploring the relationship between these parameters and cladding characteristics is the premise of laser cladding optimization.

The aim of optimization is to choose proper process parameters for the desired cladding layer. The optimization objects mainly include geometric characteristics and mechanical properties, which can be divided into single-objective optimization and multiobjective optimization. The design of experiment (DOE) is often adopted to establish empirical-statistical models between process parameters and optimization objects. Farahmand et al. [1] conducted multiobjective optimization of track height, HAZ depth, and microhardness via the response surface method (RSM) and central composite design (CCD), finally obtaining a group of optimal parameters accompanied by homogeneous chemical composition, a thick clad layer, high microhardness, and a shallow HAZ. Similarly, Yu et al. [14] determined a set of parameters corresponding to maximum track width, minimum track height, and fitted dilution by the Taguchi orthogonal experiment combined gray analysis. Meng et al. [15] built a model via RSM and ANOVA (analysis of variance) to optimize the dilution, ratio of track width to track height, and microhardness. The aforementioned studies aimed to obtain a set of optimal process parameters, but sometimes it needs to plot contour graph (i.e., process map) of interest characteristics adopting the process parameters as variables. Generally, a process map is a 2D graph whose coordinate axis is single or combined process parameters [6, 13, 16–18]. Costa et al. [16] developed a process map of track height for coating Satellite 6 on low-carbon steel; they chose low dilution (3–5%) and a big cladding angle (>100°) as limitations. With the aim of attaining the desired area (0.25 to 5 mm^2) of the track cross-section, Oliveira et al. [6] adopted the same limitations as Costa et al. [16]. The process maps developed by these studies were very convenient and effective, and they mostly concentrated on the geometric characteristics and mechanical performances, but there is a lack of research on powder efficiency and deposition speed with respect to the economic efficiency of laser cladding. For this reason, this paper focuses on the economy and efficiency optimization of laser cladding.

Based on a full factorial experiment, this study deposited Fe-based alloy powder on an AISI 1045 substrate using a 3000 W fiber laser combined with coaxial rectangular powder nozzles. A statistical analysis method was adopted to investigate the relationship between key parameters (P, V, and F) and geometric characteristics as well as the economic efficiency of single-track clad. A linear regression model was established between the combined parameter $P^{\alpha}V^{\beta}F^{c}$ and the cladding features of interest. A process map of track height was developed

Table 1: Chemical composition of AISI 1045 and Fe-based powder (wt.%).

Materials	C	Cr	Ni	Mn	Mo	Si	B	Fe
Fe-based powder	0.15	22	13	—	2	4.5	1.6	Bal.
AISI 1045	0.42	0.2	0.25	0.65	—	0.3	—	Bal.

2. Experimental Methods

Materials. AISI 1045 plate with dimensions of 300 × 100 × 10 mm^3 was employed as the substrate, which was polished and cleaned with alcohol and acetone. An Fe-based alloy powder was adopted as cladding material. The powder was prepared by gas atomization method, which has spherical shape and 53–150 μm particle size. The chemical compositions of the substrate and the powder were depicted in Table 1. Before deposition, the powder was dried for 5 hours at 120°C to ensure good fluidity [3].

Experimental Setup. Figure 1 shows the experimental setup of the laser cladding system used in this work. A 3000 W fiber laser (Precitec) with a wavelength of 1080 nm was employed. The laser head was fixed on a 6-axis KUKA robot (KR 20) as the end operator, which was driven to move relative to the workpiece placed on the worktable. The powder was blown into the melt pool via a double tank feeder rotating at 0–10 r/min. 99.99% argon was used as a powder feeding gas and shielding gas, which can prevent powder oxidation and invading metal vapor.

A single-mode laser was transformed into a rectangular uniform spot. Coaxial rectangular powder nozzles were installed symmetrically on both sides of the laser beam. The spot size and defocusing distance were 6 × 2 mm and 330 mm, respectively. The nozzle outlet size was 6 × 1.6 mm, and the tilt angle was 76°(Figure 2). Experiencing blowing and diverging, a rectangular powder spot was projected onto the substrate, where a narrow melt pool was generated (Figure 3).

Experimental Design and Analysis Method. Three key process parameters (P, V, and F) were adopted as input variables for a 3×3 factorial design experiment. According to the process parameters of diferent groups (Table 2), 27 single-clad tracks were deposited on the substrate; the length of each track was 50 mm. The flow rates of powder feeding gas and shielding gas were constant at 20 l/min and 10 l/min, respectively. The stand-of distance between the laser head and substrate was adjusted to 18 mm where the powder flow intersected to obtain the highest catchment efficiency [19].

All the tracks were cut transversely to 20 × 15 × 10 mm^3 blocks with a wire cutting machine. Each specimen was cleaned, polished, and etched. The cross-sections of the specimens were photographed by an electron microscope, and the geometry characteristics of the tracks were measured

Industrial Engineering Journal
ISSN: 0970-2555
Volume : 51, Issue 04, April : 2022

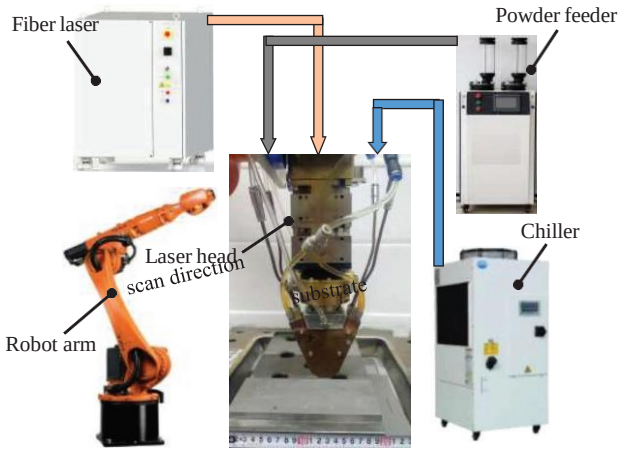

Figure 1: Schematic diagram of the laser cladding system.

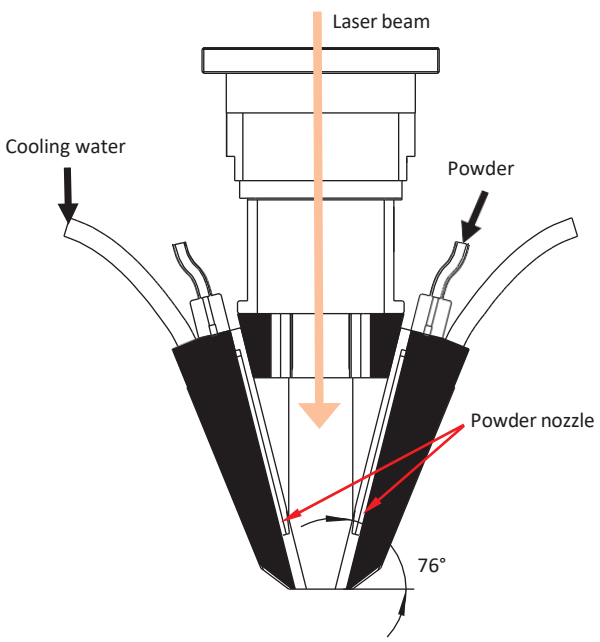

Figure 2: Structure of the laser head.

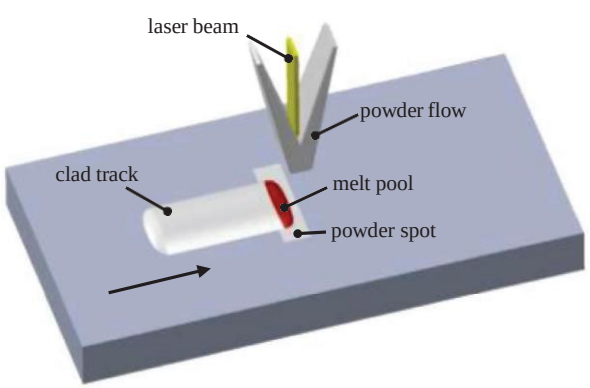

3. Results

Observing the surfaces of the tracks, it was found that all the tracks were uniform and bonded closely with the substrate. Electron microscope images showed that no cracks or pores appeared at the bonding location. Table 2 lists the values of 27 groups of process parameters and the corresponding measured data. All of the single-track cross-sections are shown in Figure 5.

Figure 3: Schematic diagram of single-track cladding.*Analysis on the Relationship between Process Parametersand Track Cross-Section*

Track Width. Measured data show that the track width of all the specimens is close to the laser spot size (6 mm); the maximum and minimum values are 5.22 mm and 6.12 mm, respectively, corresponding to *P* 1000 W, V 12 mm/s, *F* 16.5 g/min, *P* 2400 W, and V 8 mm/s, *F* 28.5 g/min. It can be concluded that wider tracks can be formed at high power, low scan speed, and high powder feed rate. Figure 6 shows that when F is constant, W_b and P present a positive and linear relationship approximately, where W_b increases as V decreases at a constant P. It may be related to the linear energy density (P/V) [6], which increases with P increases or V decreases. P/V increases mean heat absorbed by the substrate and powder per unit length increases, and more material will melt to generate a larger melt pool, resulting in W_b increasing. Compared with Figure 6(a), 6(b), and 6(c), it is found that F has little efect on W_b, while P and V are the main factors afecting W_b.

Track Height. Figure 7 depicts the variation trend of H_b with F and V. H_b increases as F increases; there is an approximate linear positive correlation between them, and Figure 7(b) presents a perfect linear relationship. H_b increases dramatically, especially at high power and low scan speed (V 8 mm/s in Figure 7(c)), and the in- creasing rate (maximum value/minimum value) is up to 172%. H_b increases as V decreases, and the increase rate is up to 180% when V is reduced from 12 mm/s to 8 mm/s (Figure 7(c)). It can be concluded that both F and V have remarkable efects on H_b, and the combined parameters F/V can give a reasonable explanation. F/V means powder feeding mass per unit length [6]. F/V increases with F increases or V decreases, so more powder could be injected into the melt pool, leading to a higher clad track. Figure 7 also shows that P has little efect on H_b.

Industrial Engineering Journal
ISSN: 0970-2555
Volume : 51, Issue 04, April : 2022

Table 2: Geometry parameters, corresponding powder efficiency (η), and deposition speed (D_s) of all the 27 clad tracks at diferent process parameters.

No	Process parameters			Geometry parameters of cross-section				Economical indexes	
	P (W)	V (mm/s)	F (g/min)	W_b (mm)	H_b (mm)	A_b (mm^2)	θ (°)	η (%)	D_s (mm^3/s)
1#	1800	8	16.5	5.56	0.52	2.05	153.5	46.87	16.4
2#	1800	10	16.5	5.43	0.26	1.08	151.5	30.87	10.8
3#	1800	12	16.5	5.22	0.24	0.88	163.5	30.18	10.56
4#	2100	8	16.5	5.81	0.42	1.78	153.2	40.70	14.24
5#	2100	10	16.5	5.73	0.34	1.48	158.8	42.30	14.8
6#	2100	12	16.5	5.58	0.23	0.93	151.0	31.90	11.16
7#	2400	8	16.5	5.94	0.46	2.01	156.6	45.96	16.08
8#	2400	10	16.5	5.91	0.35	1.61	156.9	46.02	16.1
9#	2400	12	16.5	5.83	0.27	1.26	159.6	43.22	15.12
10#	1800	8	22.5	5.61	0.54	2.23	155.0	37.39	17.84
11#	1800	10	22.5	5.46	0.4	1.57	157.5	32.91	15.7
12#	1800	12	22.5	5.29	0.29	1.11	161.0	27.92	13.32
13#	2100	8	22.5	5.91	0.56	2.48	141.9	41.58	19.84
14#	2100	10	22.5	5.74	0.42	1.85	154.9	38.78	18.5
15#	2100	12	22.5	5.56	0.32	1.32	161.2	33.20	15.84
16#	2400	8	22.5	6.09	0.58	2.65	151.3	44.44	21.2
17#	2400	10	22.5	5.90	0.44	2.03	151.3	42.55	20.3
18#	2400	12	22.5	5.71	0.37	1.62	155.6	40.75	19.44
19#	1800	8	28.5	5.58	0.73	2.93	146.2	38.79	23.44
20#	1800	10	28.5	5.41	0.51	1.94	156.6	32.10	19.4
21#	1800	12	28.5	5.13	0.36	1.34	159.3	26.61	16.08
22#	2100	8	28.5	5.81	0.69	2.97	149.4	39.32	23.76
23#	2100	10	28.5	5.62	0.50	2.08	148.0	34.42	20.8
24#	2100	12	28.5	5.45	0.41	1.63	153.5	32.37	19.56
25#	2400	8	28.5	6.12	0.79	3.54	144.4	46.86	28.32
26#	2400	10	28.5	6.02	0.60	2.64	150.7	43.69	26.4
27#	2400	12	28.5	5.68	0.44	1.88	153.3	37.33	22.56

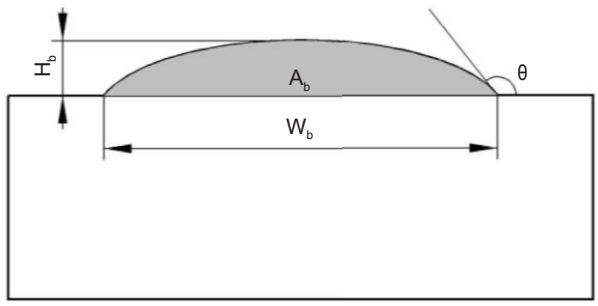

Figure 4: Schematic diagram of the track cross-section.

process parameters deciding θ as previous analysis. Because the track cross-section is neither a regular arc or ellipse nor is it symmetrical, the measured data are not precise enough [13], so the cladding angle is not discussed much in this work.

Analysis of Profiles of the Track Cross-Section. In order to improve cladding efficiency, the tracks generated by wide-band laser are wider than round spot laser (Figure 3), so the profiles of track cross-sections are long and narrow, consequently θ is large enough to avoid defects. According to the photographs in Figure 5, the tracks mainly changed in bulged height with diferent process parameters. H_b varies more remarkable and has much larger increasing rate (261%) than W_b (119%), therefore the former has moresignificant efect on track shape.

Considering the influence of W_b and H_b, the ratio of W_b to H_b [10, 15] (R) was adopted to characterize the track profile in this paper. As shown in Figure 7, nine samples were chosen to explain the evolution of the track profiles. No. 19# sample has the smallest R due to the highest H_b, it also has the most remarkable arc profile. When R is 13.7 (14# in Figure 8), it becomes to appear a flat-top feature of the contours. As R increases, the rest of the tracks almost have the same characteristic. No. 6# sample has the biggest R but H_b is too low to meet cladding requirements. Taking the simplicity of calculation and diferent contexts into consideration, many research adopted arc or parabolic for profile fitting [20, 21], but it is not applicable in this paper. As shown in Figure 9(a), ellipse fitting is performed on the same photographs in Figure 8. Apparently, ellipse fits well to most of the tracks especially to which has low R value (upper photographs in Figure 9(a)). But it is worth noting that the curve doesn't stay so close to the top of the contour any more with R increasing (lower photographs in Figure 9(a)), so a variation trend was given in Figure 9(b). The minor axis gradually de-

Industrial Engineering Journal
ISSN: 0970-2555
Volume : 51, Issue 04, April : 2022

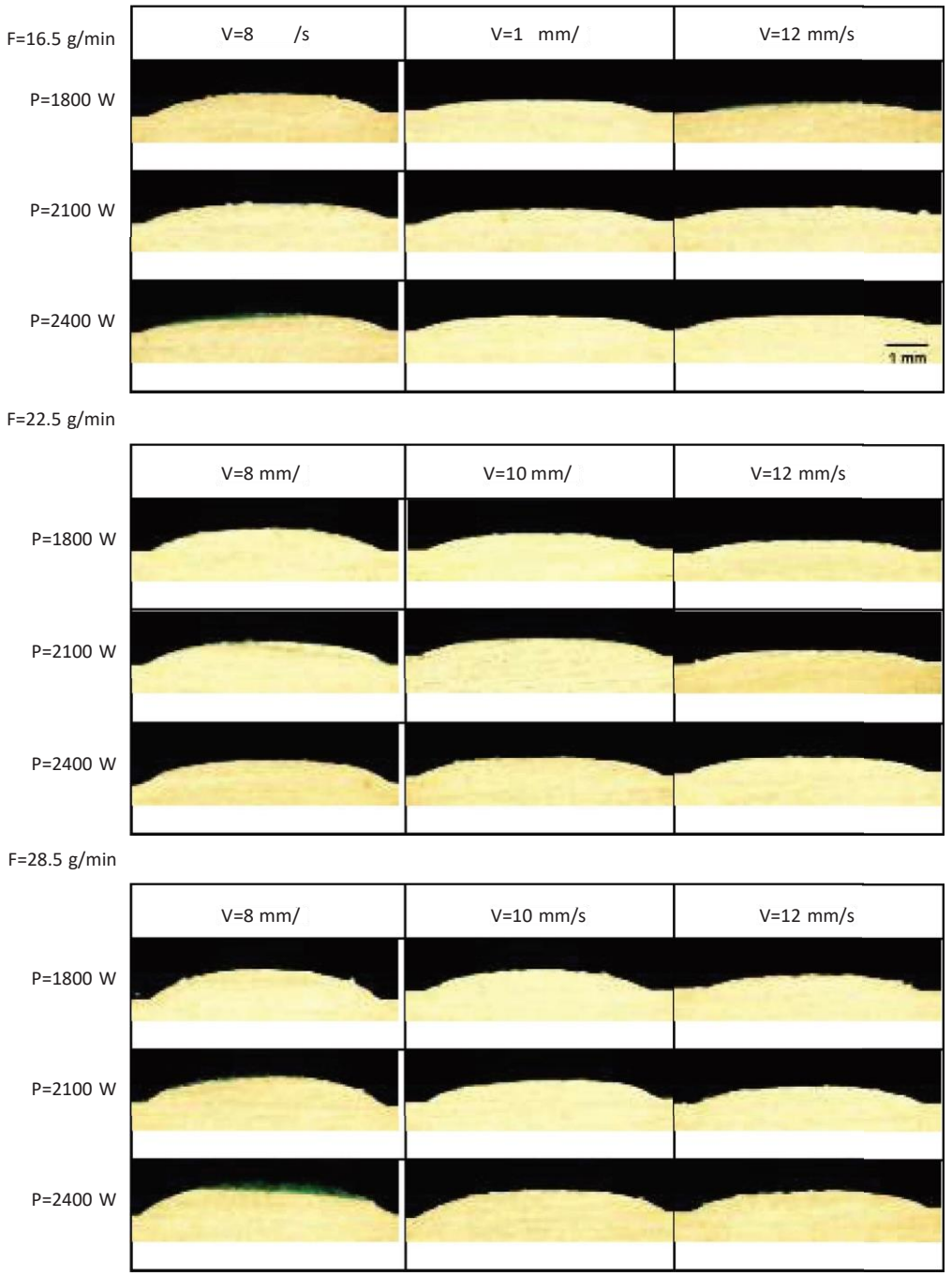

Figure 5: All of the 27 single-track cross-sections. For each powder feed rate (F), the scan speed (V) increases from left to right and the laser power (P) increases from top to bottom.

Observing Figure 5, it is found that the flat-top feature is more predominant with high scan speed, P and F have little efect on the flat-top feature. The underlying mechanism of the flat-top feature will not been discussed in this work, but this special characteristic can be utilized to achieve a good surface evenness if the

Analysis of Key Economy Indexes. Powder efficiency refers to the ratio of melted powder to feeding powder, assuming that the cross-sections of tracks are uniform along the scan direction, the powder efficiency η can be expressedas

$$\eta = \frac{\rho A_b V}{F} \times 100\%, \qquad (1)$$

Industrial Engineering Journal
ISSN: 0970-2555
Volume : 51, Issue 04, April : 2022

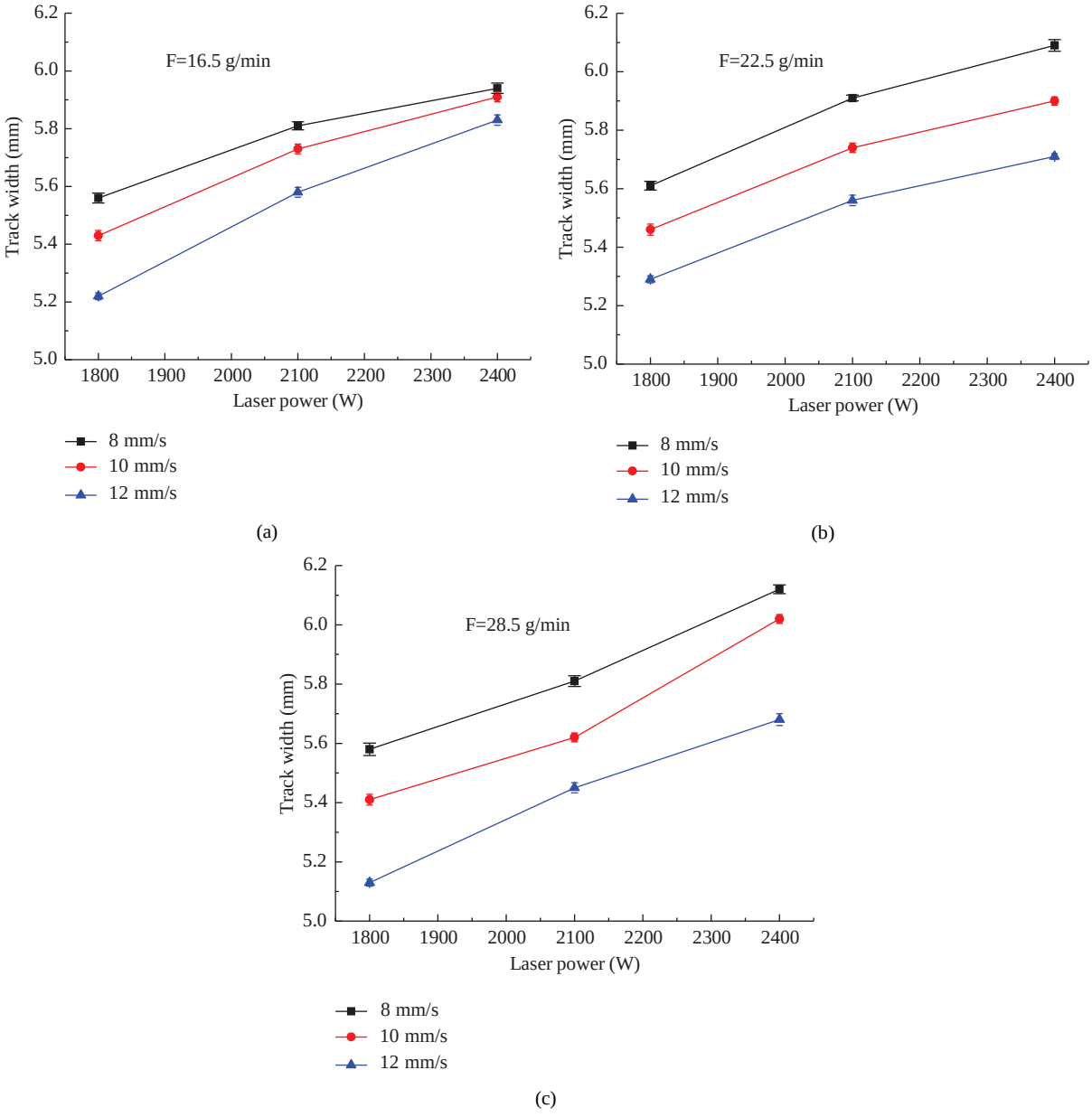

Figure 6: Variation of track width with laser power and scan speed at given powder feed rate. (a) F = 16.5 g/min; (b) F = 22.5 g/min; (c) F = 28.5 g/min.

where ρ is the powder density (7.86 g/cm^3), A_b is area of the track cross-section (mm^2). The calculated η ranges from 20%–50% (Table 2). Lower η corresponded to small laser power and high scan speed, and higher η was derived from big laser power and low scan speed. This may be subjected to the relationship between P/V and F, low P/V accompanied with high F would diminish the melt pool area leads to less powder trapped in the melt pool. It not only reduces the powder efficiency, but also generates powder adhesion on the track surface. On the contrary, when P/V increases or F decreases, the melt pool area would be enlarged and more powder been melted

resulting in higher powder efficiency. Figure 10 depicts how η changes with V and F at P 1800 W and 2400 W, η has a downward trend as F increases. Especially when V 8 mm/s, F increases from 16.5 g/min to 22.5 g/min, there is a

Industrial Engineering Journal
ISSN: 0970-2555
Volume : 51, Issue 04, April : 2022

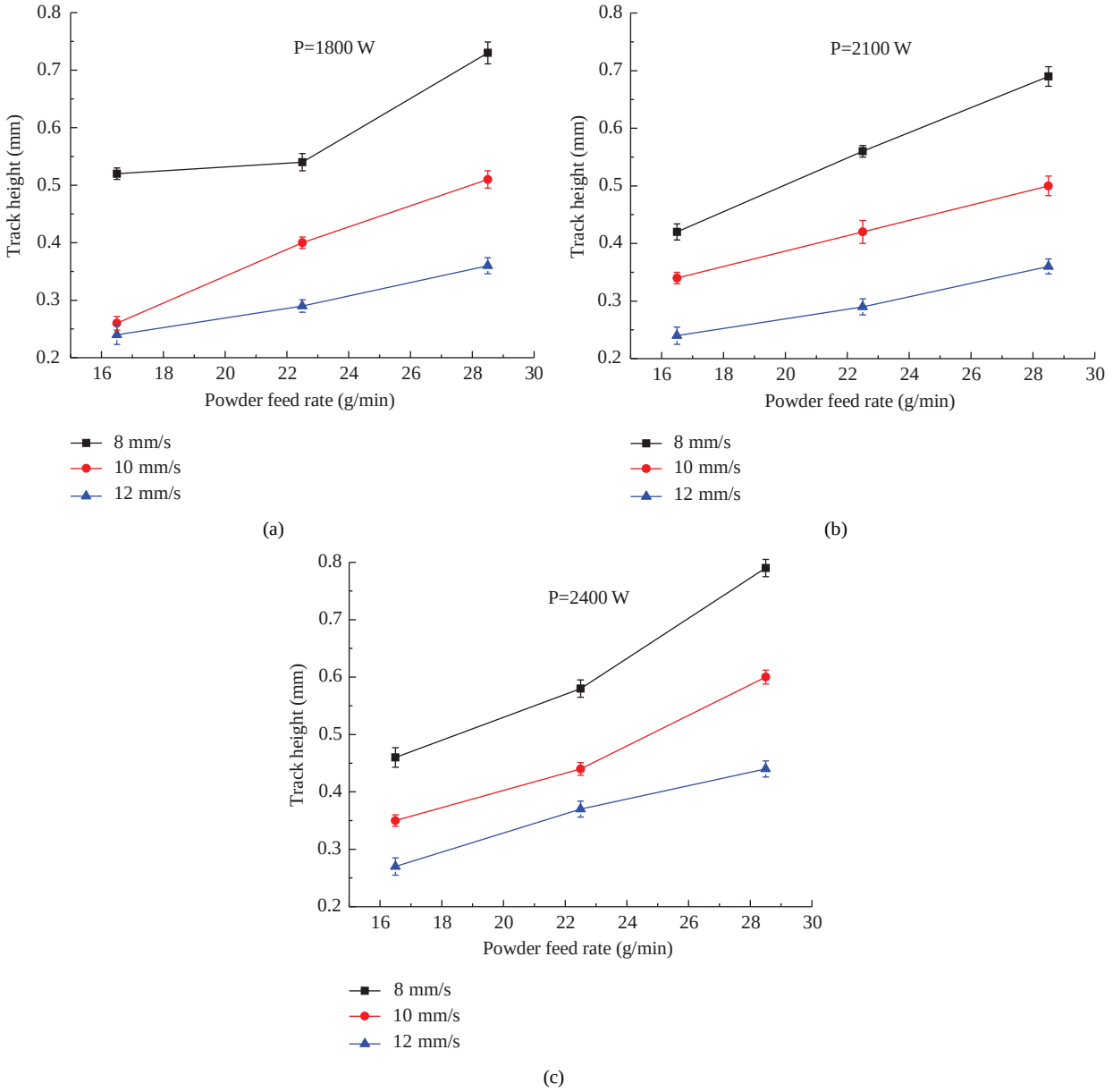

Figure 7: Variation of track height with powder feed rate and scan speed at given laser power. (a) *P* = 1800 W; (b) *P* = 2100 W; (c) *P* = 2400 W.

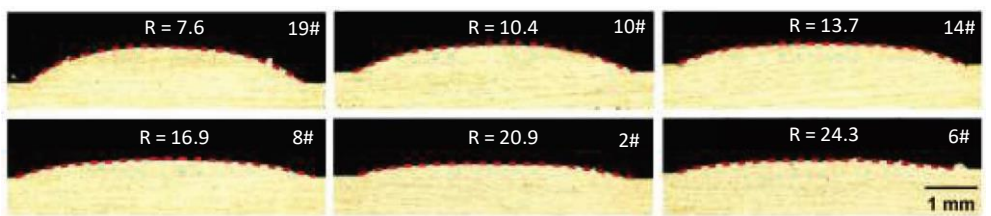

Figure 8: Contours of the track cross-section with diferent R (the ratio of W_b to H_b). The upper right number of each photograph is consistent with Table 2.

Industrial Engineering Journal
ISSN: 0970-2555
Volume : 51, Issue 04, April : 2022

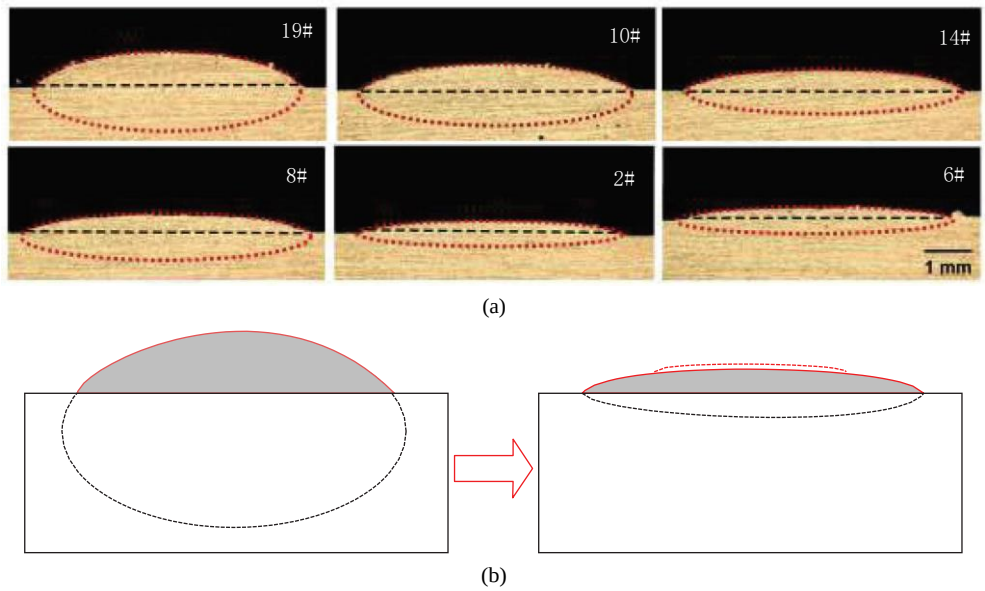

Figure 9: Ellipse fitting of the track cross-section. (a) Ellipses of diferent tracks (the upper right number of each photograph is consistent with Table 2); (b) the deformation tendency of the fitting curves.

where V_b is track volume (mm^3). As formula (2) depicts, D_s increases with V, but when P is constant, D_s reduces rapidly as V decreases (Figures 10(c) and 10(d)); therefore, V has a negative efect on D_s. Both H_b and W_b decrease with V (Figures 6 and 7), resulting in a smaller A_b, so D_s will decrease quickly, and the positive efects of V are counteracted. In addition, when P and V are constant, the laser line energy density (P/V) and powder feed weight per unit length (F/V) will decrease as V increases, as does D_s. Figures 10(c) and 10(d) also shows that when V is constant, D_s increases sharply with F because more powder are trapped in the melt pool. It can be concluded that D_s depends strongly on the geometric characteristics of clad tracks, and P, V, and F all have significant efects on D_s.

Process Optimization for Economy Efciency

Empirical Model. As discussed earlier, both η and D_s mainly depend on the geometric characteristics of clad tracks; however, simple combined parameters (P/V and F/V) are not adequate to describe the relationship between process parameters and economic efficiency [13]. Therefore, according to the method proposed by Benjamin et al. [13], an empirical model was established between combined parameters and economic efficiency as well as the geometric characteristics of the clad tracks. The linear regression expression of the model is $y = a(P^{\alpha}V^{\beta}F^{c}) + b$, where y is certain respond of interest; P, V, and F represent laser power, scan speed, and powder feed rate; each value of α, β, and c represents the significance on y; a and b are slope and intercept of the linear equation, respectively. In this work, linear fitting was performed between combined parameters $P^{\alpha}V^{\beta}F^{c}$ and H_b, R, η and D_s, the results are shown in Figure 11.

As shown in Figure 11(a), in equation y = 0.653x-0.315, where y represents H_b, x represents combined parameters $V^{-3/4}F^{3/5}$, P is not included because it has little efect on H_b. The exponent of V is negative means that V has a negative efect on H_b, likewise, F has a positive efect on H_b due to the positive exponent. The combined parameters and H_b have a good fitting degree R^2 = 0.92. In Figure 11(b), the combined parameters also do not include P, indicating that P has no significant efect on R, V has a positive efect on R and F has a negative efect on R, which is consistent with the views of Qian et al. [10] and Meng et al. [15]. Because the absolute values of the exponents belong to V and F are equal, they have the same efects on R. Since R^2 of H_b and R are impressive enough, it can be concluded that P, V, and F are the key process parameters afecting the geometric characteristics.

F has a negative efect on η and is far less significant than P and V (Figure 11(c)); this coincides well with the analysis of 3.3. The R^2 of η is 0.76 indicating a low fitting degree, probably because there are other significant process parameters not been considered, such as stand-ofdistance between nozzle and substrate, flow rate of delivery gas, structure of powder feeder and so on [6, 19, 20]. D_s has linear relationship with $P^{2/5}V^{-2/5}F^{3/4}$ (Figure 11(d)), V has negative efect on D_s, which coincides well with Section 3.3, the fact that F has the highest exponent means it has the most significant efect on D_s. R^2 of η and D_s are not as impressive

Industrial Engineering Journal
ISSN: 0970-2555
Volume : 51, Issue 04, April : 2022

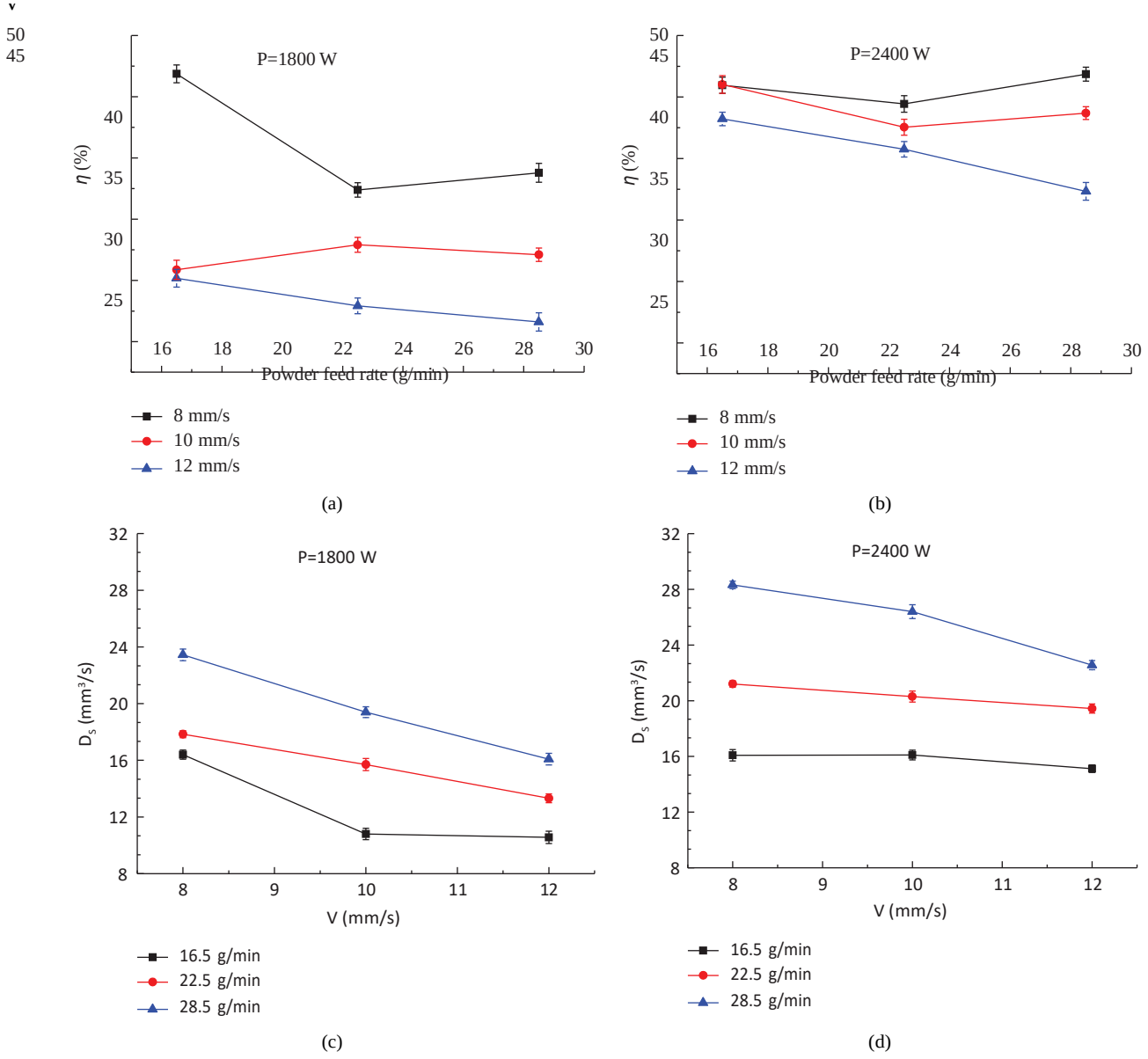

Figure 10: Efect of process parameters on powder efficiency (η) and deposition speed (D_s). (a, c) are at a constant power 1800 W. (b, d) are at a constant power 2400 W.

usually damages the coating quality due to too much mixed substrate materials. According to Tuominen et al. [4] and Turichin et al. [5], a low dilution rate (lower than 10%) can be easily achieved by a high-power fiber laser with a wide-band laser, so unlike other studies, this work did not consider dilution as a boundary any more. The convexity of a single-clad track determines the bonding quality of adjacent cladding and the surface evenness of the cladding layer. Bulging too much may cause unmelted defects or pores, and in turn, the desired layer thickness cannot be achieved if the convex is too low. So as described in Section 3.2, R was adopted as a boundary of the clad track shape. Since most powders are expensive, improving powder efficiency is significant for reducing the costs of additive manufacturing. Additionally, increasing deposition speed is an efective means to reduce production costs, which is more urgent for additive manufacturing. Therefore, η and D_s were determined as optimization objects. H_b was chosen as a tailored geometry characteristic, which was usually adopted by process maps in previous studies [16, 17, 22].

In this work, considering the experimental results, R 6 and R 18 were defined as track shape boundaries, η 50% and D_s 20 mm^3/s were chosen as the lowest limitations of economic efficiency. As P has positive efects on η and D_s (Figure 11(c) and 11(d)), so a constant value 2800 W was determined. Then, plotted 2D process map, taking V and F

Industrial Engineering Journal
ISSN: 0970-2555
Volume : 51, Issue 04, April : 2022

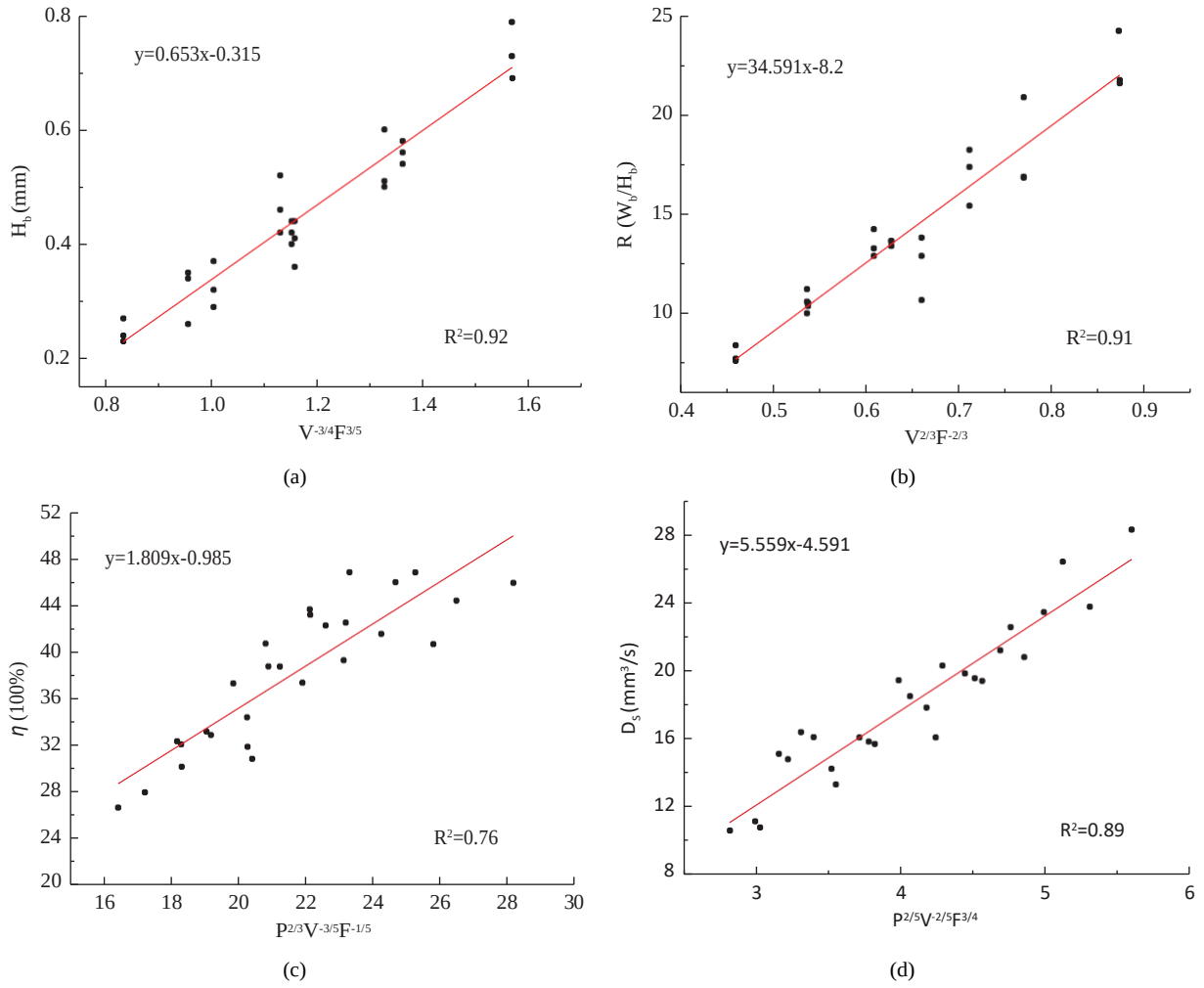

Figure 11: Linear fitting relationship between combined parameters and the bead characteristics: (a) H_b. (b) R. (c) η. (d) D_s.

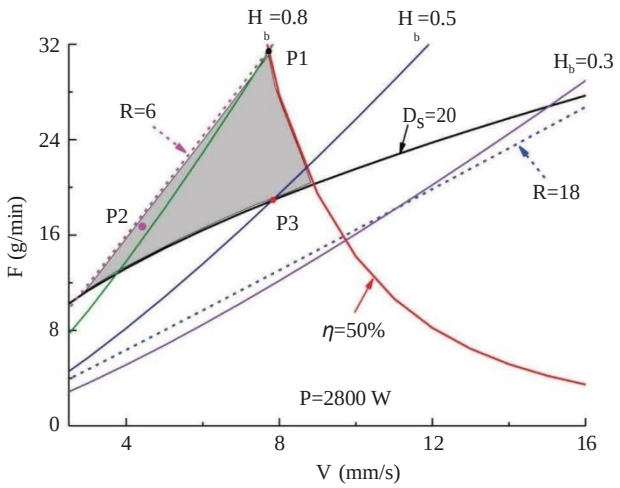

contour lines of H_b 0.3, 0.5, and 0.8 mm were painted according to the corresponding linear model.

As shown in Figure 12, the left zone of the contour η 50% has a higher powder efficiency than 50%, and the upper zone of the contour D_s 20 has a higher deposition speed than 20 mm^3/s. The three curves R 6, η 50%, and D_s 20 formed a triangular zone (i.e., an operation window) where arbitrary points can be chosen to obtain high powder efficiency and deposition speed as well as good clad quality. Table 3 lists the coordinate values (F, V), tailored geometry values, and optimization results of three diferent points (P1, P2, and P3 marked in Figure 12) chosen in the operation window. It should be emphasized that the curve H_b 0.3 completely locates outside of the operation window; high D_s can be achieved with high V value but resulting in low η. Both H_b 0.5 and H_b 0.8 curves are partly in the operation window, and the latter has a wider value range. It can be

Industrial Engineering Journal
ISSN: 0970-2555
Volume : 51, Issue 04, April : 2022

Table 3: Optimization results of diferent points (P1, P2, and P3) chosen in the operation window of Figure 12.

NO.	V (mm/s)	F (g/min)	H_b (mm)	D_s (mm^3/s)	H (%)
P1	7.7	31.4	0.8	>20	50%
P2	4.4	16.7	>0.8	>20	>50%
P3	7.8	19	0.5	20	>50%

4. Discussion

Confined to the laser spot size, W_b is close to 6 mm in this paper. The laser spot width used to be wider than 10 mm in order to improve the cladding speed [3, 23]. H_c is mainly decided by powder feeding mass per unit length (F/V) if the powder melts well, so the thickness of the cladding layer can be controlled by altering F or V. According to formulas (1) and (2), η and D_s can be improved by increasing A_c at constant F and V; thus, η and D_s increased impressively as P increased from 1800 W to 2400 W (Figure 10); this means the laser should work at nominal power to achieve high η and D_s.

Ellipse fitting coincides well with the profile of the single-track cross-section, but there still exists a little deviation due to the flat-top feature (Figure 9). Some researchers strove to predict the profiles according to process parameters (P, V, and F) to avoid high costs and time-consuming experiments, but their numerical models were based on the premise that the profiles were subjected to simple functions such as arc, parabolic, hyperbolic, or sinusoidal [3, 20–24]. The functions were very applicable in their respective situations but had no universality; maybe a more accurate solution is to calculate the height of each point in the contour. An efective method is to solve the integration of powder instantaneous concentration against melting time [20, 25].

It is worth noting that the R^2 values of η and D_s are not so impressive as expected. There may be other vital factors not considered except for P, V, and F. Although the powder in the melt pool can be completely melted at optimized process parameters (P, V, and F), but inevitably there is still a part of powder that falls outside of the melt pool due to scattering. This part of the powder is blown away by the feeding gas or bounced of the substrate; the more this part of powder, the lower the powder efficiency. Therefore, factors that influence the powder concentration must be taken into account for powder efficiency. Powder convergence is mainly decided by the geometric parameters and stand-of distance of the powder nozzle. As for a coaxially symmetric rectangular nozzle, exit width, chamber length, and inclination angle all have efects on the powder flow distribution and convergence [26], and the highest powder concentration emerges at the intersection of the powder flow [27]. Powder concentration will decrease as the laser head leaves from the substrate, and a high feeding gas flow is beneficial to powder aggregation [27]. The low powder efficiency in this work (Table 1) was not only related to P, V, and F but also subjected to the powder nozzle. F has an impressive efect on D_S (exponent is 3/4 in Figure 11(d)); given that P, V, and F are held constant, there is no doubt that D_s can be improved by increasing η. Therefore, the factors influencing η also act on D_s indirectly, resulting in a low R^2 of D_s. For the sake of high powder efficiency and deposition speed, it is equally vital to optimize the process parameters (P, V, and F) and geometric parameters of the powder nozzle.

5. Conclusions

According to DOE and statistical analysis, a linear regression model was established between the combined parameters ($P^{\alpha}V^{\beta}F^{c}$) and the clad geometry (H_b, R) as well as economic efficiency (η, D_s). The exponent of P, V, and F means significance and positive or negative association. R^2 of each function (H_b, R, η, and D_s) was 0.91, 0.92, 0.76, and 0.89, respectively. R^2 of η and D_s were not impressive because the geometric parameters of powder nozzle also had significant efects on powder concentration. Enhancing powder convergence not only can improve powder efficiency but also increase deposition speed indirectly. Proper boundaries were determined to plot a 2D process map with a constant power of 2800 W. In the operation window, the powder efficiency could reach more than 50%, and the deposition speed could reach more than 20 mm^3/s.

Data Availability

The experiment data used to support the findings of this study are included within the article.

Conflicts of Interest

The authors declare that there are no conflicts of interest regarding the publication of this paper.

References

[1] P. Farahmand and R. Kovacevic, "Parametric study and multi-criteria optimization in laser cladding by a high power direct diode laser," *Lasers Manuf. Mater. Process*, vol. 1, no. 1-4, pp. 1–20, 2014.

[2] S. Liu, F. Kong, S. Shi, and R. Kovacevic, "Study of a hollow laser beam for cladding," *International Journal of Advanced Manufacturing Technology*, vol. 73, no. 1-4, pp. 147–159, 2014.

[3] H. Liu, X. Qin, S. Huang, Z. Hu, and M. Ni, "Geometry modeling of single track cladding deposited by high power diode laser with rectangular beam spot," *Optics and Lasers in Engineering*, vol. 100, pp. 38–46, 2018.

[4] J. Tuominen, J. Näkki, H. Pajukoski et al., "Laser cladding with 15 kW fiber laser," in *Proceedings of the 13th NOLAMP Conference in Trondheim*, pp. 27–29, Trondheim, January

[5] U. De Oliveira, V. Ocelik, and J. T. M. De Hosson, "Analysis of coaxial laser cladding processing conditions," *Surface and Coatings Technology*, vol. 197, no. 2-3, pp. 127–136, 2005.
[6] D. M. Goodarzi, J. Pekkarinen, and A. Salminen, "Efect of process parameters in laser cladding on substrate melted areas and the substrate melted shape," *Journal of Laser Applications*, vol. 27, no. S2, 2015.
[7] J. Ju, Y. Zhou, M. Kang, and J. Wang, "Optimization of process parameters, microstructure, and properties of laser cladding fe-based alloy on 42CrMo steel roller," *Materials*, vol. 11, no. 10, p. 2061, 2018.
[8] N. Sommer, F. Stredak, and S. Böhm, "High-speed laser cladding on thin-sheet-substrates - influence of process parameters on clad geometry and dilution," *Coatings*, vol. 11, no. 8, p. 952, 2021.
[9] M. Qian, L. C. Lim, Z. D. Chen, and W. I. Chen, "Parametric studies of laser cladding processes," *Journal of Materials Processing Technology*, vol. 63, no. 1-3, pp. 590–593, 1997.
[10] A. Riquelme, P. Rodrigo, M. D. Escalera-Rodr´ıguez, and J. Rams, "Analysis and optimization of process parameters in Al–SiCp laser cladding," *Optics and Lasers in Engineering*, vol. 78, pp. 165–173, 2016.
[11] K. Benarji, Y. R. Kumar, C. P. Paul, A. N. Jinoop, and K. S. Bindra, "Parametric investigation and characterization on SS316 built by laser-assisted directed energy deposition," *Proceedings of the Institution of Mechanical Engineers - Part L: Journal of Materials: Design and Applications*, vol. 234, no. 3, pp. 452–466, 2020.
[12] B. Bax, R. Rajput, R. Kellet, and M. Reisacher, "Systematic evaluation of process parameter maps for laser cladding and directed energy deposition," *Additive Manufacturing*, vol. 21, pp. 487–494, 2018.
[13] T. Yu, L. Yang, Y. Zhao, J. Sun, and B. Li, "Experimental research and multi-responsemulti-parameter optimization of laser cladding Fe313," *Optics & Laser Technology*, vol. 108, pp. 321–332, 2018.
[14] G. Meng, L. Zhu, J. Zhang, Z. Yang, and P. Xue, "Statistical analysis and multi-objective process optimization of laser cladding TiC-Inconel718 composite coating," *Optik*, vol. 240, Article ID 166828, 2021.
[15] L. Costa, I. Felde, T. Reti et al., "A simplified semi-empirical method to select the processing parameters for laser clad coatings," *Materials Science Forum*, vol. 414-415, pp. 385–394, 2003.
[16] P. Shayanfar, H. Daneshmanesh, and K. Janghorban, "Parameters optimization for laser cladding of inconel 625 on ASTM A592 steel," *Journal of Materials Research and Technology*, vol. 9, no. 4, pp. 8258–8265, 2020.
[17] M. Ansari, R. Shoja Razavi, and M. Barekat, "An empirical-statistical model for coaxial laser cladding of NiCrAlY powder on Inconel 738 superalloy," *Optics & Laser Technology*, vol. 86, pp. 136–144, 2016.
[18] H. K. Lee, "Efects of the cladding parameters on the deposition efficiency in pulsed Nd:YAG laser cladding," *Journal of Materials Processing Technology*, vol. 202, pp. 321–327, 2008.
[19] H. El Cheikh, B. Courant, S. Branchu, J. Y. Hascoet, and R. Guillén, "Analysis and prediction of single laser tracks geometrical characteristics in coaxial laser cladding process," *Optics and Lasers in Engineering*, vol. 50, no. 3, pp. 413–422, 2012.
[20] H. Tian, X. Chen, Z. Yan, X. Zhi, Q. Yang, and Z. Yuan, "Finite-element simulation of melt pool geometry and

Industrial Engineering Journal
ISSN: 0970-2555
Volume : 51, Issue 04, April : 2022